Electronic Supplementary Information

Pressure-driven structural phase transition and metallization in two-dimensional ferromagnetic semiconductor $CrBr_3$

Meiling Hong,[a] Lidong Dai,*[a] Haiying Hu,*[a] Xinyu Zhang,[ab] Chuang Li[ab] and Yu He[ab]

[a]Key Laboratory of High-Temperature and High-Pressure Study of the Earth's Interior, Institute of Geochemistry, Chinese Academy of Sciences, Guizhou 550081, China;

[b]University of Chinese Academy of Sciences, Beijing 100049, China

*Corresponding authors

Emails: L. D. Dai (dailidong@vip.gyig.ac.cn) and H. Y. Hu (huhaiying@vip.gyig.ac.cn)

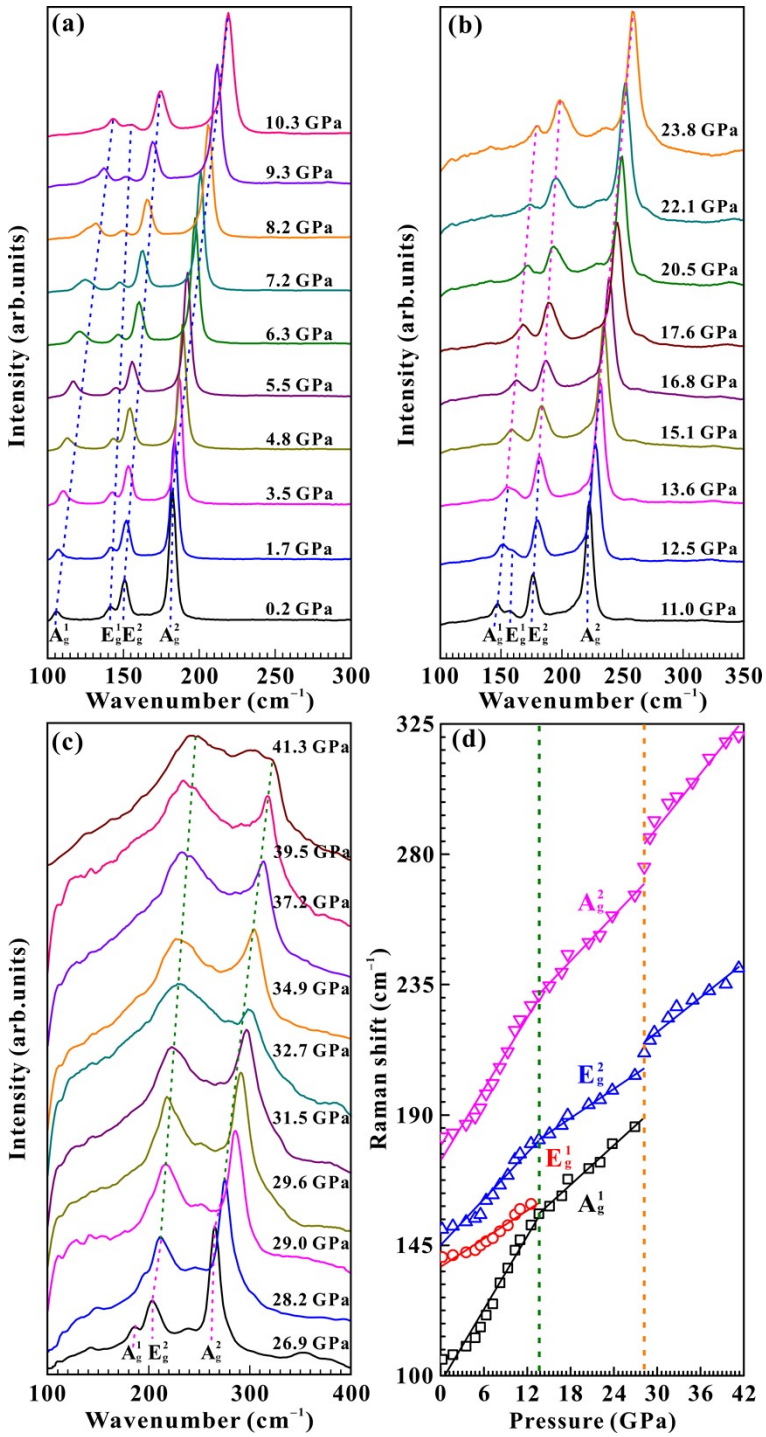

Fig. S1 (a)−(c) High-pressure Raman spectroscopy of $CrBr_3$ within the pressure range of 0.2−41.3 GPa during pressurization. (d) Pressure-dependent Raman shifts for $CrBr_3$ under hydrostatic condition. Errors in Raman wavenumber are within the size of the symbol.

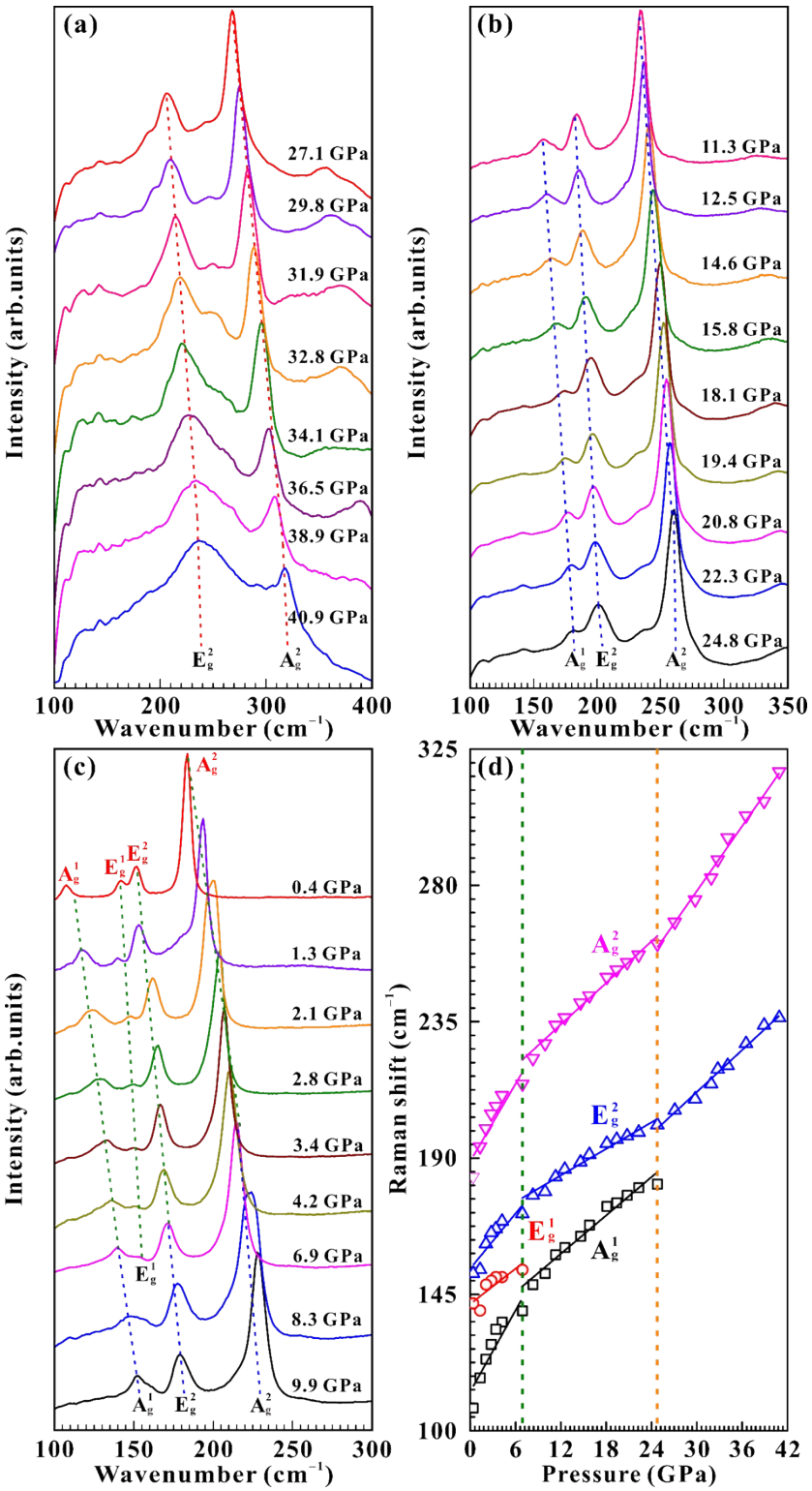

Fig. S2 (a)−(c) High-pressure Raman spectroscopic results on $CrBr_3$ within the pressure range of 40.9−0.4 GPa during decompression. (d) The evolution of Raman shifts versus pressure under hydrostatic condition.

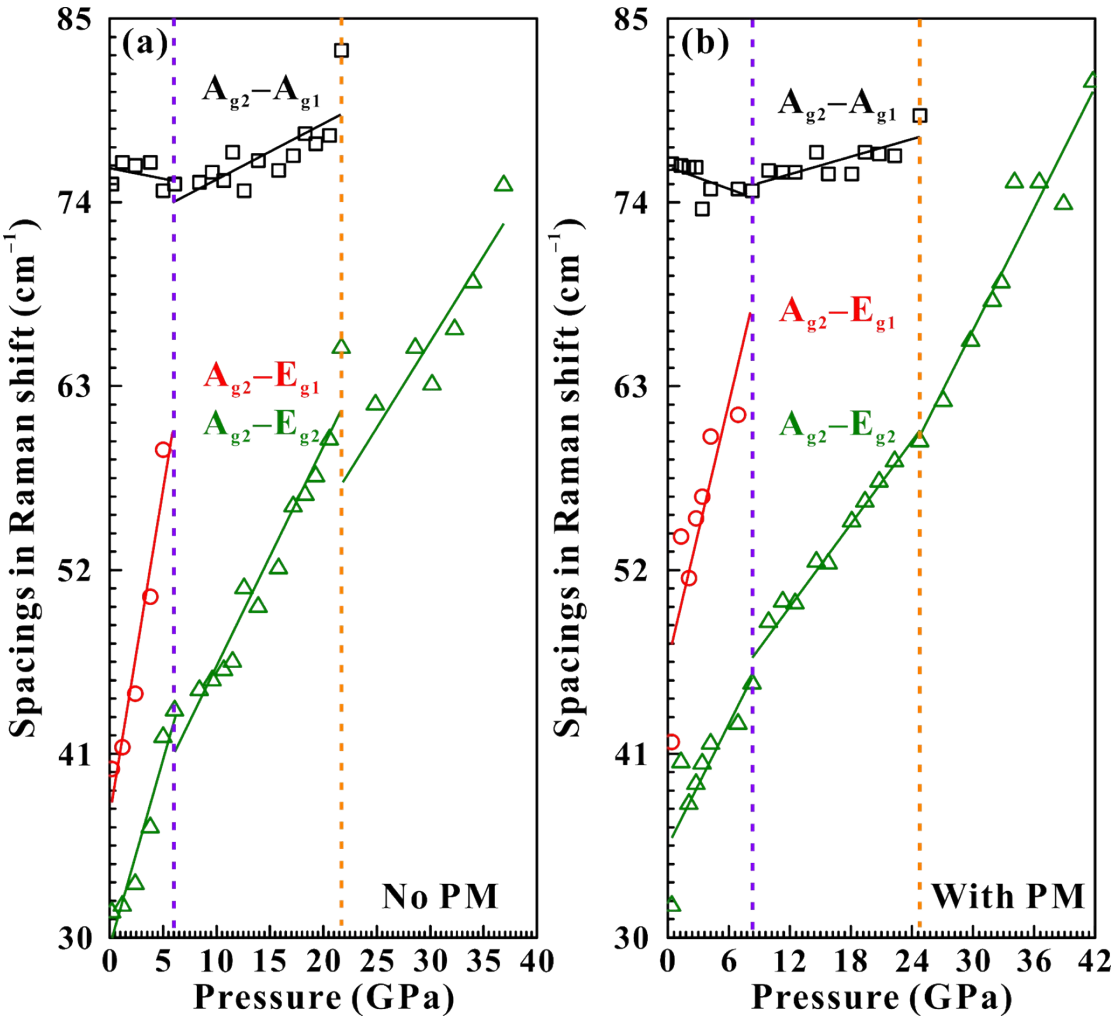

Fig. S3 Pressure dependence of the spacings in Raman shifts for $CrBr_3$ under (a) non-hydrostatic condition and (b) hydrostatic condition during the process of decompression. PM refers to the pressure medium.

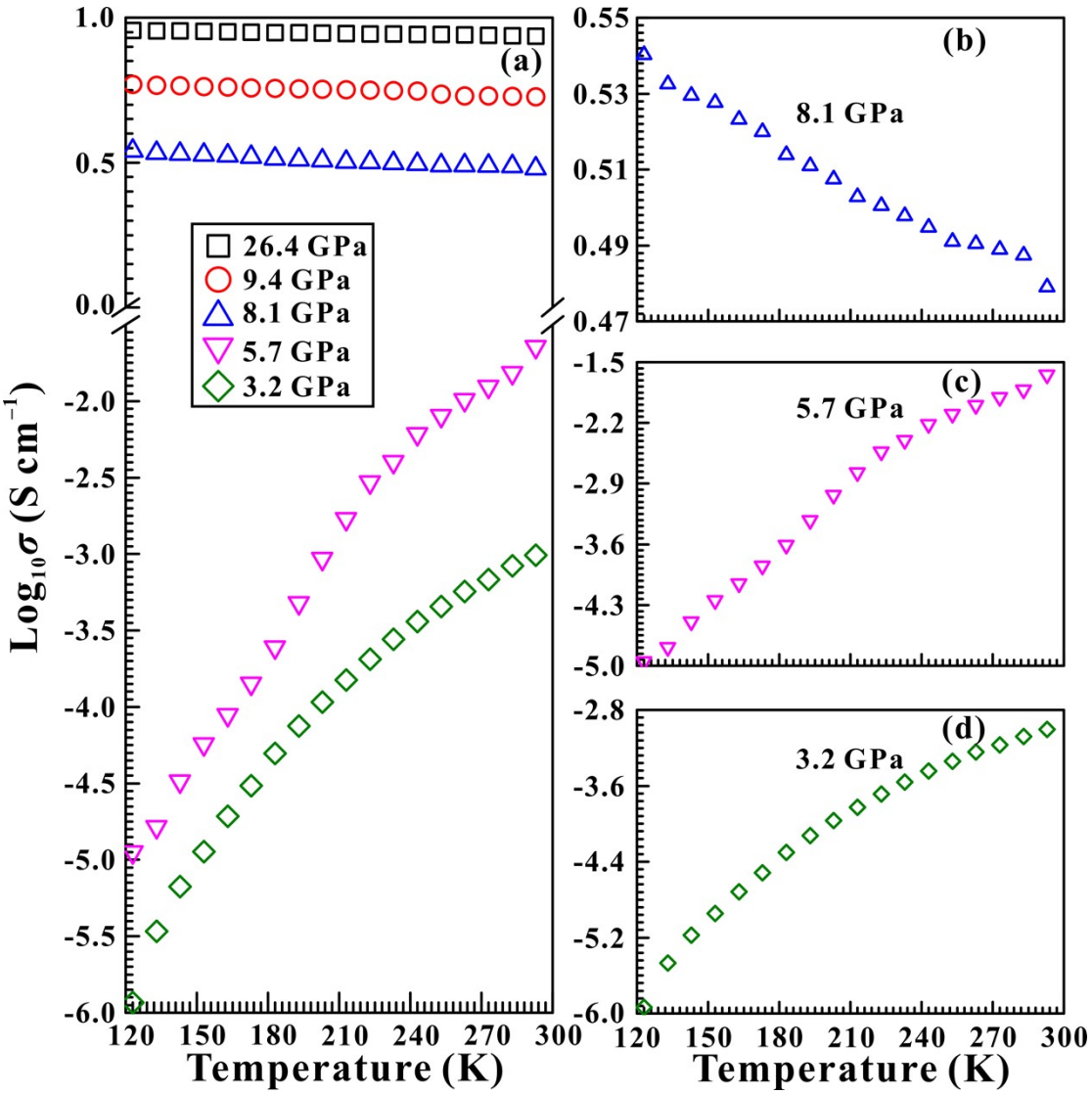

Fig. S4 The variable-temperature electrical conductivity experiments of $CrBr_3$ at some typical pressures. Herein, (a) denotes all results at pressures of 26.4, 9.4, 8.1, 5.7 and 3.2 GPa during decompression; (b) denotes the metallic feature of sample at 8.1 GPa; (c) denotes the semiconducting property of $CrBr_3$ at 5.7 GPa and (d) denotes the semiconducting behavior of sample at 3.2 GPa, respectively.

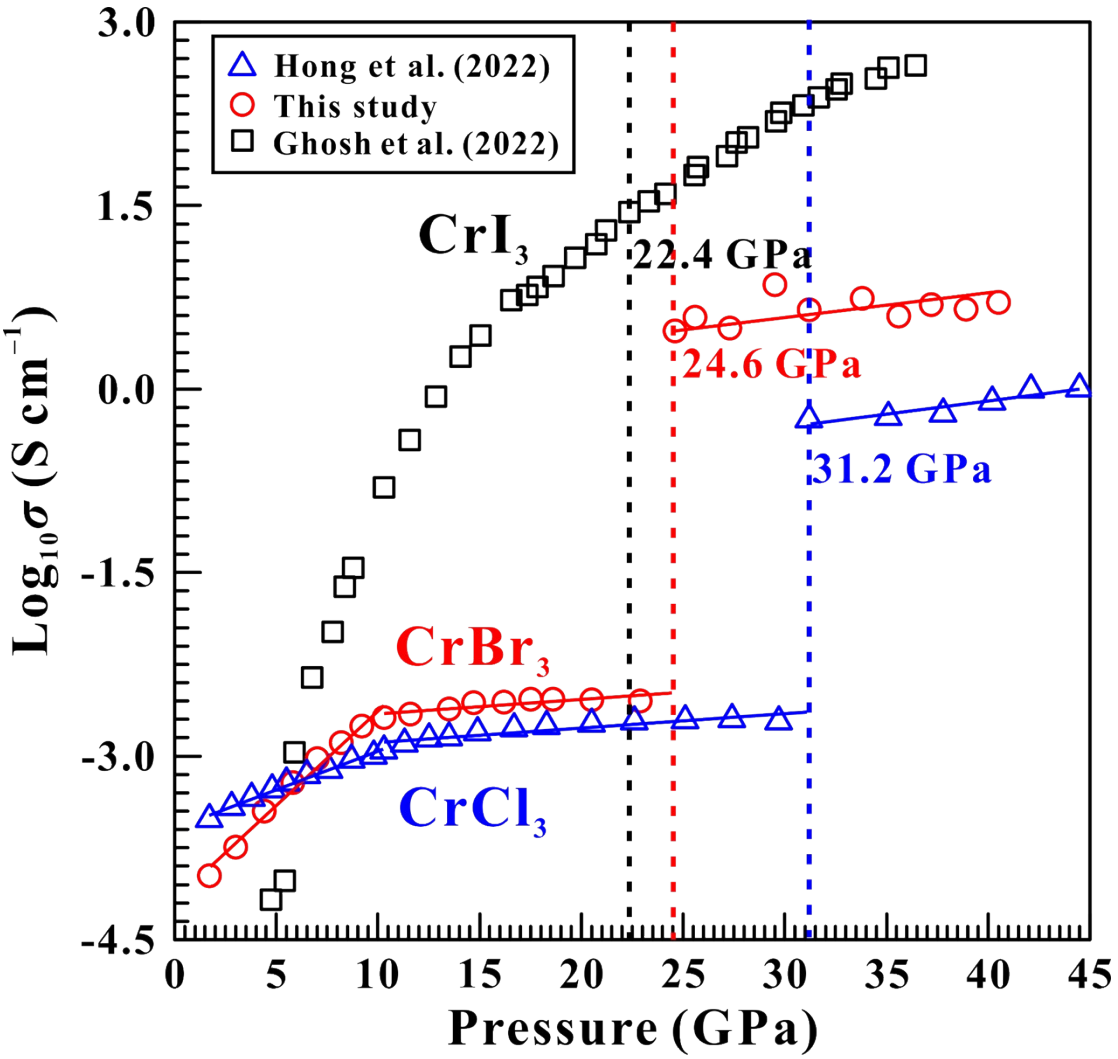

Fig. S5 The evolution of electrical conductivity as a function of pressure for CrX_3 (X = Cl, Br and I) compounds at atmospheric temperature upon pressurization.

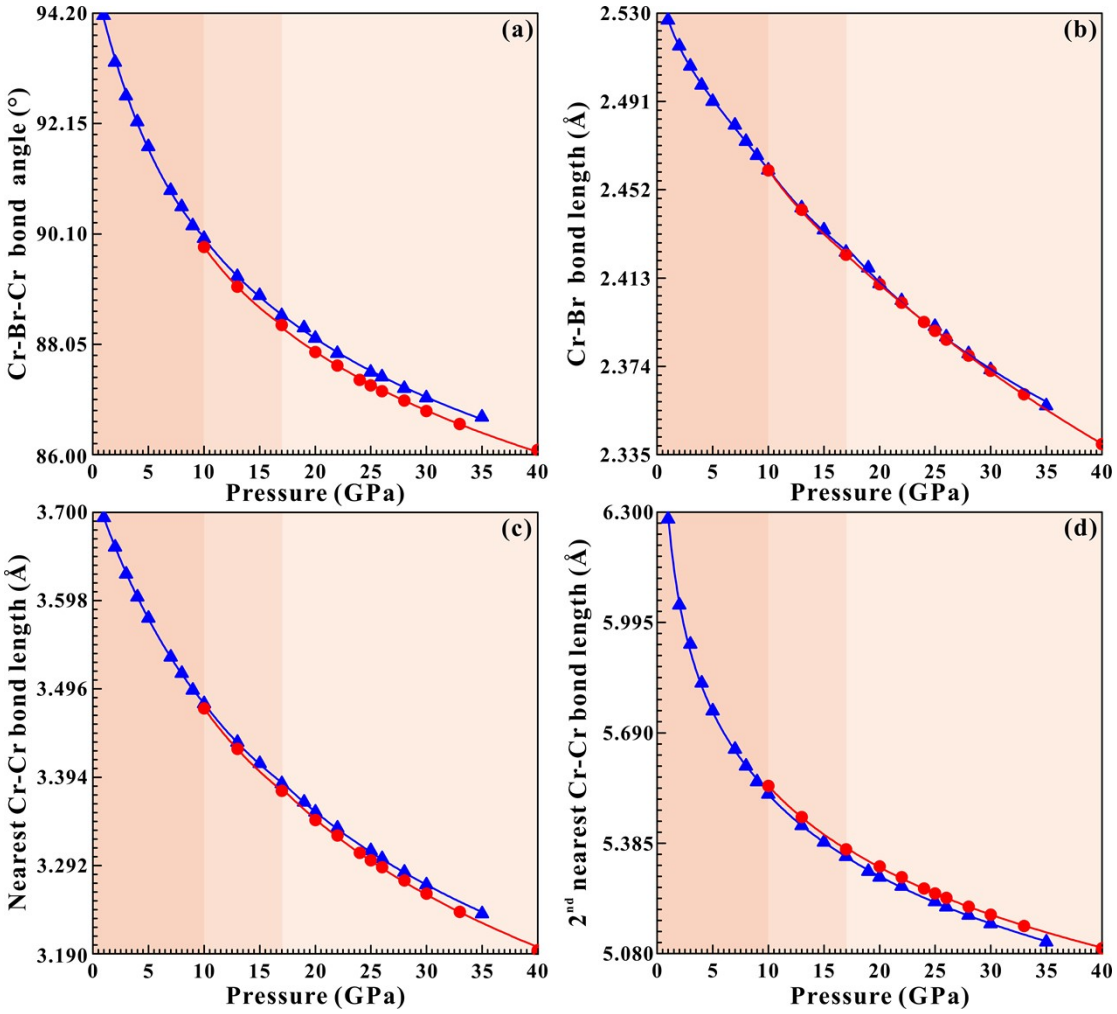

Fig. S6 Theoretical calculation results on (a) Cr-Br-Cr bond angle; (b) Cr-Br bond length; (c) nearest Cr-Cr bond length and (d) 2nd nearest Cr-Cr bond length for the ferromagnetic $CrBr_3$ phase and the metallic M12 phase within the pressure range of 1–40 GPa. In here, the solid bule triangles stand for the results of the ferromagnetic $CrBr_3$ phase and the solid red circles represent the results of the M12 phase of $CrBr_3$ under high pressure, respectively.

Table S1. Pressure-dependent Raman shift ($d\omega/dP$, $cm^{-1}\ GPa^{-1}$) for $CrBr_3$ under non-hydrostatic and hydrostatic environments upon compression and decompression. Here, ω (cm^{-1}) and P (GPa) represent the Raman frequency and pressure, respectively.

Pressure condition		Pressure (GPa)	ω (cm^{-1})	$d\omega/dP$ ($cm^{-1}\ GPa^{-1}$)	ω (cm^{-1})	$d\omega/dP$ ($cm^{-1}\ GPa^{-1}$)
Non-hydrostatic	Compression	0.9–9.5	105.8 (A_g^1)	4.66	136.5 (E_g^1)	1.94
			148.3 (E_g^2)	2.89	182.7 (A_g^2)	4.62
		9.5–25.9	142.8 (A_g^1)	3.04	–	–
			171.6 (E_g^2)	2.05	219.8 (A_g^2)	3.31
		25.9–37.6	–	–	–	–
			204.2 (E_g^2)	2.26	274.5 (A_g^2)	3.38
	Decompression	36.9–21.7	–	–	–	–
			216.0 (E_g^2)	1.23	291.0 (A_g^2)	1.86
		21.7–5.0	181.4 (A_g^1)	2.78	–	–
			199.2 (E_g^2)	1.83	264.5 (A_g^2)	3.09
		5.0–0.2	135.5 (A_g^1)	6.12	151.0 (E_g^1)	2.14
			168.2 (E_g^2)	3.91	210.2 (A_g^2)	6.04
Hydrostatic	Compression	0.2–13.6	105.6 (A_g^1)	4.22	141.0 (E_g^1)	1.62
			150.5 (E_g^2)	2.65	182.5 (A_g^2)	4.11
		13.6–28.2	155.9 (A_g^1)	2.27	–	–
			181.4 (E_g^2)	1.68	231.5 (A_g^2)	2.62
		28.2–41.3	–	–	–	–
			211.4 (E_g^2)	1.98	275.6 (A_g^2)	3.00
	Decompression	40.9–24.8	–	–	–	–
			236.3 (E_g^2)	2.31	317.5 (A_g^2)	3.57
		24.8–6.9	181.4 (A_g^1)	2.30	–	–
			200.9 (E_g^2)	1.58	260.6 (A_g^2)	2.47
		6.9–0.4	139.6 (A_g^1)	4.84	153.1 (E_g^1)	1.95
			171.6 (E_g^2)	3.24	214.4 (A_g^2)	4.53

Table S2. Pressure dependence of Raman full width at half maximum (FWHM) (dF/dP, cm^{-1} GPa^{-1}) for $CrBr_3$ under non-hydrostatic and hydrostatic environments upon pressurization. In here, ω (cm^{-1}), F (cm^{-1}) and P (GPa) stand for the Raman frequency, Raman FWHM and pressure, respectively.

Pressure condition	Pressure (GPa)	ω (cm^{-1})	F (cm^{-1})	dF/dP (cm^{-1} GPa^{-1})	ω (cm^{-1})	F (cm^{-1})	dF/dP (cm^{-1} GPa^{-1})
Non-hydrostatic	0.9–9.5	105.8 (A_g^1)	5.87	0.26	136.5 (E_g^1)	4.22	1.28
		148.3 (E_g^2)	4.93	0.39	182.7 (A_g^2)	4.79	0.32
	9.5–25.9	142.8 (A_g^1)	9.10	−0.67	–	–	–
		171.6 (E_g^2)	8.12	0.36	219.8 (A_g^2)	7.49	0.27
	25.9–37.6	–	–	–	–	–	–
		204.2 (E_g^2)	16.9	2.38	274.5 (A_g^2)	12.2	−0.22
Hydrostatic	0.2–13.6	105.6 (A_g^1)	4.16	0.37	141.0 (E_g^1)	7.23	0.52
		150.5 (E_g^2)	4.29	0.23	182.5 (A_g^2)	4.44	0.20
	13.6–28.2	155.9 (A_g^1)	13.7	−0.62	–	–	–
		181.4 (E_g^2)	7.58	0.39	231.5 (A_g^2)	6.73	0.15
	28.2–41.3	–	–	–	–	–	–
		211.4 (E_g^2)	14.2	1.32	275.6 (A_g^2)	9.15	−0.32

Table S3. The spacings in Raman shift against pressure (dS/dP, cm^{-1} GPa^{-1}) for $CrBr_3$ under non-hydrostatic and hydrostatic environments during both processes of compression and decompression. In here, S (cm^{-1}) and P (GPa) are the spacings in Raman shift and pressure, respectively.

Pressure condition		Pressure (GPa)		S (cm^{-1})	dS/dP (cm^{-1} GPa^{-1})		S (cm^{-1})	dS/dP (cm^{-1} GPa^{-1})
Non-hydrostatic	Compression	0.9–9.5	A_g^2–A_g^1	76.9	−0.042	A_g^2–E_g^1	46.2	2.99
			A_g^2–E_g^2	34.4	1.72	–	–	–
		9.5–25.9	A_g^2–A_g^1	77.0	0.26	–	–	–
			A_g^2–E_g^2	48.2	1.27	–	–	–
		25.9–37.6	–	–	–	–	–	–
			A_g^2–E_g^2	70.3	0.68	–	–	–
	Decompression	36.9–21.7	–	–	–	–	–	–
			A_g^2–E_g^2	75.0	0.63	–	–	–
		21.7–5.0	A_g^2–A_g^1	83.1	0.31	–	–	–
			A_g^2–E_g^2	65.3	1.26	–	–	–
		5.0–0.2	A_g^2–A_g^1	74.7	−0.078	A_g^2–E_g^1	59.2	3.91
			A_g^2–E_g^2	42.0	2.13	–	–	–
Hydrostatic	Compression	0.2–13.6	A_g^2–A_g^1	76.9	−0.098	A_g^2–E_g^1	41.5	2.44
			A_g^2–E_g^2	32.0	1.46	–	–	–
		13.6–28.2	A_g^2–A_g^1	75.6	0.29	–	–	–
			A_g^2–E_g^2	50.1	0.93	–	–	–
		28.2–41.3	–	–	–	–	–	–
			A_g^2–E_g^2	64.2	0.94	–	–	–
	Decompression	40.9–24.8	–	–	–	–	–	–
			A_g^2–E_g^2	81.2	1.26	–	–	–
		24.8–6.9	A_g^2–A_g^1	79.2	0.17	–	–	–
			A_g^2–E_g^2	59.7	0.89	–	–	–
		6.9–0.4	A_g^2–A_g^1	74.8	−0.30	A_g^2–E_g^1	61.3	2.59
			A_g^2–E_g^2	42.8	1.29	–	–	–

Table S4. The comparisons of the high-pressure structural transition and metallization pressures for CrX_3 (X = Cl, Br and I) compounds under non-hydrostatic and hydrostatic environments upon compression and decompression. In here, P_{tr} and P_m are the structural transition and metallization pressures of CrX_3 compounds.

Materials		Pressure conditions	1^{st} P_{tr} (GPa)	2^{nd} P_{tr} (GPa)	P_m (GPa)	References
$CrCl_3$	Compression	Non-hydrostatic	10.0	28.0	–	Ahmad et al. (2020)
	Compression	Non-hydrostatic	9.9	29.8	31.2	Hong et al. (2022)
		Hydrostatic	11.7	32.2	–	
$CrBr_3$	Compression	Non-hydrostatic	9.5	25.9	24.6	This study
		Hydrostatic	13.6	28.2	–	
	Decompression	Non-hydrostatic	5.0	21.7	–	
		Hydrostatic	6.9	24.8	–	
CrI_3	Compression	Non-hydrostatic	–	–	22.4	Ghosh et al. (2022)